Human Molecular Genetics, 2022, Vol. 31, No. 4 548–560

https://doi.org/10.1093/hmg/ddab267
Advance Access Publication Date: 11 September 2021
Original Article

ORIGINAL ARTICLE

The vitamin A transporter STRA6 adjusts the stoichiometry of chromophore and opsins in visual pigment synthesis and recycling

Srinivasagan Ramkumar[1,†], Vipul M. Parmar[1], Ivy Samuels[2], Nathan A. Berger[3,4], Beata Jastrzebska[1,5] and Johannes von Lintig[1,*,‡]

[1]Department of Pharmacology, School of Medicine, Case Western Reserve University, Cleveland, OH 44106, USA, [2] Northeast Ohio VA Healthcare System, Cleveland, OH 44106, USA, [3]Center for Science, Health and Society, School of Medicine, Case Western Reserve University, Cleveland, OH 44106, USA, [4]Case Comprehensive Cancer Center, Case Western Reserve University, Cleveland, OH 44106, USA and [5]Cleveland Center for Membrane and Structural Biology, School of Medicine, Case Western Reserve University, Cleveland, OH 44106, USA

*To whom correspondence should be addressed at: Department of Pharmacology (W341), School of Medicine, Case Western Reserve University, 10900 Euclid Avenue, Cleveland, OH 44106, USA. Tel: +1 2163683528; Fax: +1 2163681300; Email: johannes.vonlintig@case.edu

Abstract

The retinal pigment epithelium of the vertebrate eyes acquires vitamin A from circulating retinol binding protein for chromophore biosynthesis. The chromophore covalently links with an opsin protein in the adjacent photoreceptors of the retina to form the bipartite visual pigment complexes. We here analyzed visual pigment biosynthesis in mice deficient for the retinol-binding protein receptor STRA6. We observed that chromophore content was decreased throughout the life cycle of these animals, indicating that lipoprotein-dependent delivery pathways for the vitamin cannot substitute for STRA6. Changes in the expression of photoreceptor marker genes, including a downregulation of the genes encoding rod and cone opsins, paralleled the decrease in ocular retinoid concentration in STRA6-deficient mice. Despite this adaptation, cone photoreceptors displayed absent or mislocalized opsins at all ages examined. Rod photoreceptors entrapped the available chromophore but exhibited significant amounts of chromophore-free opsins in the dark-adapted stage. Treatment of mice with pharmacological doses of vitamin A ameliorated the rod phenotype but did not restore visual pigment synthesis in cone photoreceptors of STRA6-deficient mice. The imbalance between chromophore and opsin concentrations of rod and cone photoreceptors was associated with an unfavorable retinal physiology, including diminished electrical responses of photoreceptors to light, and retinal degeneration during aging. Together, our study demonstrates that STRA6 is critical to adjust the stoichiometry of chromophore and opsins in rod and cone photoreceptors and to prevent pathologies associated with ocular vitamin A deprivation.

[†]Srinivasagan Ramkumar, http://orcid.org/0000-0002-2542-1501
[‡]Johannes von Lintig, http://orcid.org/0000-0002-2079-2143
Received: July 28, 2021. **Revised:** September 2, 2021. **Accepted:** September 3, 2021

Introduction

Vitamin A (all-*trans*-retinol, ROL) must be distributed to the eyes to support photoreceptor function in the retina (1). But the hydrophobicity of retinoids presents a physical barrier for simple aqueous diffusion. Therefore, vertebrates have evolved specific protein-assisted transport mechanisms to distribute the fat-soluble vitamin within the body in a coordinated fashion (2).

Dietary vitamin A precursors are absorbed by intestinal enterocytes and metabolically converted to retinyl esters (REs). REs are transported, along with other dietary lipids, in triacylglycerol-rich chylomicrons (3). The remainder in chylomicron remnants is deposited in the liver and stored in hepatic stellate cells (4,5).

Hepatic vitamin A is released as RE in very low-density lipoproteins (6,7). Peripheral tissues can render RE available from different lipoprotein classes in a lipoprotein lipase-dependent manner (8). Additionally, the liver secretes ROL bound to the retinol-binding protein (RBP) (2,9). Holo-RBP is the major retinoid in the fasting circulation and forms a complex with the 55 kDa transthyretin (10). Although ROL exchanges between RBP and membranes (11), the existence of RBP receptor in the retina pigment epithelium (RPE) was reported in biochemical studies (12). Later, the receptor was molecularly identified as stimulated by retinoic acid 6 gene product (STRA6) (13,14). Cellular accumulation of ROL via STRA6 is driven by conversion to RE catalyzed by lecithin:retinol acyltransferase (LRAT) activity (15,16). In the RPE, REs are converted into chromophore to support visual pigment synthesis and recycling in an enzyme-mediated pathway called the visual cycle (17,18) (Fig. 1A).

Humans and mice with loss of function mutations in the *RBP* gene thrive and only display a mild ocular phenotype (9,19,20). Knockout mice deficient for STRA6 were also generated in several laboratories (21–23). Similar to RBP-deficient mice, *Stra6*$^{-/-}$ mice display a reduced ocular vitamin A concentration and impaired electrical responses of rod and cone photoreceptors to light early in life (21,22,24). Ocular vitamin A concentrations increase during adolescence but STRA6-deficient mice are vulnerable to dietary vitamin A deprivation (21,25).

These observations led to the proposal that peripheral tissues including the eyes receive the vitamin through both lipoprotein and RBP-dependent delivery pathways (26) (Fig. 1A). It was further proposed that the pathways are complementary and that only when all delivery pathways fail peripheral tissues will suffer from vitamin A deficiency (7).

The molecular identification and biochemical characterization of STRA6 challenged this view on vitamin A transport. Studies in cell lines indicate that STRA6 acts as a bidirectional vitamin A transporter, suggesting an active role of the transporter in adjusting retinoid tissue levels (15,16). Recent studies revealed that calcium and calmodulin can influence the direction of the flux of ROL between cellular and extracellular compartments (27). Mounting evidence also indicate that the activity of STRA6 in extraocular tissues is subject to transcriptional regulation by retinoid signaling (28,29). However, the role of STRA6 in ocular vitamin A uptake homeostasis is still understudied.

We previously showed in mice that the activity of STRA6 varies depending on tissue type and supply condition of dietary vitamin A (21,25). We now scrutinized the role of STRA6 in ocular vitamin A uptake homeostasis. By comparing STRA6-deficient eyes to the eyes of control mice under high supply conditions for the vitamin, we studied the impact of the RBP receptor on visual pigment biosynthesis and photoreceptor function. The picture that emerged is that STRA6 is critical for these processes and that the mouse eyes display characteristic features of ocular vitamin A deficiency in the absence of the vitamin A transporter. We further showed that the unfavorable retina physiology of STRA6-deficient mice was associated with abridged responses of photoreceptors to light at all ages and that it triggered retinal degeneration during aging. Together, our study demonstrates that STRA6 plays a crucial role in maintaining the stoichiometry between chromophore and opsins in visual pigment synthesis and establishes STRA6 as an essential component in vertebrate vision.

Results

Effects of STRA6 mutation on ocular retinoids

STRA6 is expressed in the RPE to support vitamin A uptake for chromophore synthesis and recycling (Fig. 1A). We first examined how the depletion of STRA6 influences the ocular retinoid concentration during adolescence by normal phase high performance chromatography (HPLC) analyses and compared these results to wild-type (WT) mice (Fig. 1B). In 1-month-old *Stra6*$^{-/-}$ mice, the ocular retinoid concentration was 14% of that of age-matched WT mice. During adolescence, ocular retinoid concentrations progressively increased in *Stra6*$^{-/-}$ mice to reach a maximum of approximately 400 pmol per eye at 8 months of age (50% of the content of WT mice). Ocular retinoid concentrations then plateaued until mice reached an age of 16 months (Fig. 1B). The same trend as for the total retinoid concentration was observed for the individual retinoid cycle intermediates, such as 11-*cis*-RAL, all-*trans*-retinal (atRAL) and ROL (Fig. 1C and D). Notably, RE levels were particularly low at all ages in the STRA6-deficient mice (Fig. 1C and D). Thus, STRA6-deficient mice displayed highly decreased ocular retinoid concentrations early in life, which increased during adolescence. However, ocular retinoid concentrations never reached the concentrations of age-matched WT mice (Fig. 1B). In the following experiments, we focused on two ages, 1 and 8 months, to assess the consequences of this phenotype on photoreceptor biology.

Expression of cone- and rod-specific transcription factors

Photoreceptor cell fate is determined by a network of transcription factors (30–32). To test whether the *Stra6* genotype affected the expression of these genes, we examined the mRNA levels of cone- and rod-specific transcription factors in 1- and 8-month-old *Stra6*$^{-/-}$ mice and compared them to age-matched WT mice. For rod photoreceptors, we choose the genes encoding cone-rod homeobox (*Crx*), neural retina leucine zipper (*Nrl*) and photoreceptor-specific nuclear receptor (*Nr2e3*). For cone photoreceptors, we choose genes encoding Kruppel-like transcription factors *Klf4* and *Klf9*. The analyses revealed that the mRNA levels of the rod-specific marker genes, *Crx* and *Nrl*, were 2-fold lower in 1-month-old *Stra6*$^{-/-}$ mice when compared to age-matched WT mice. No significant differences were observed for the *super family 2 group E member 3* (*Nr2e3*) gene at this age. At 8 months of age, the mRNA levels of *Crx* and *Nrl* became indistinguishable from WT mice, whereas the expression level of *Nr2e3* gene was slightly lower at this age when compared to WT mice (Fig. 2A–F). Analyses of the mRNA expression levels of the cone-specific marker genes revealed a different outcome. *Klf4* mRNA level was 2-fold higher in 1-month-old *Stra6*$^{-/-}$ mice and 2-fold higher in 8-month-old *Stra6*$^{-/-}$ mice compared to the levels in WT mice (Fig. 2G and H). Levels of *Klf9* did not

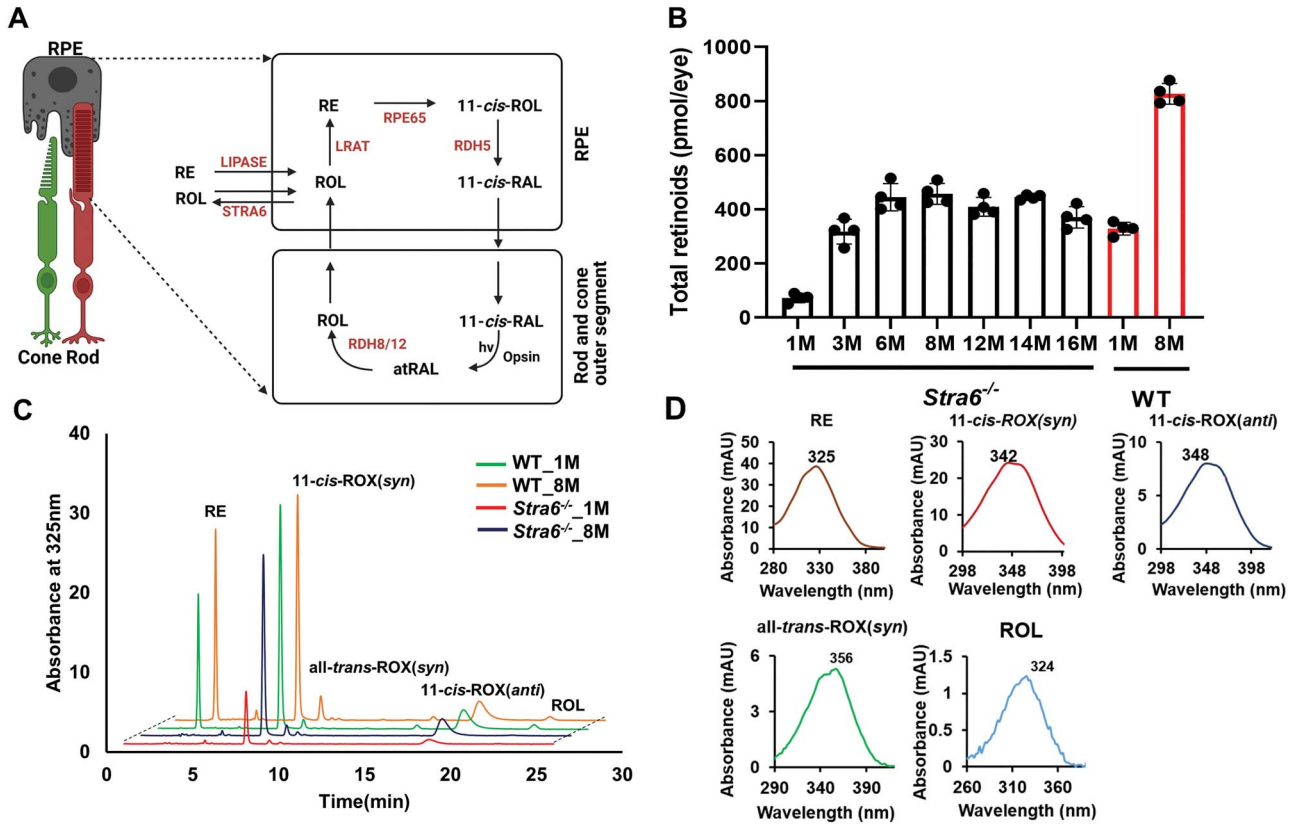

Figure 1. Ocular retinoid concentration and composition in *Stra6*$^{-/-}$ and WT mice. (**A**) Scheme of the visual cycle. RAL, retinaldehyde, RDH, retinal dehydrogenase, ROL, retinol, RPE65, retinoid isomerase. (**B**) Total ocular retinoid content of *Stra6*$^{-/-}$ and WT mice at different ages. (**C**) HPLC traces at 325 nm of ocular retinoid extracts of 1- and 8-month-old *Stra6*$^{-/-}$ and WT mice. The peaks for the individual ocular retinoids are indicated in the figure. Note that different retinal diastereomers were converted to the corresponding retinal oximes (ROX) during the extraction which exist as *syn* and *anti* isomers. (**D**) Spectral characteristics of individual ocular retinoids.

display a significant differential expression between *Stra6*$^{-/-}$ mice and age-matched WT mice (Fig. 2I and J). Thus, our analysis discovered apparent differences between *Stra6*$^{-/-}$ and WT mice in the expression of transcription factors determining rod and cone photoreceptor cell fate (Fig. 2).

Rod and cone opsin expression in *Stra6* $^{-/-}$ mice

Rod and cone photoreceptors express specific opsins, rhodopsin (encoded by *Rho* gene) in rods, and M-opsin (encoded by the *Opn1mw* gene) and S-opsin (encoded by the *Opn1sw* gene) in cones (33). We next determined the expression levels of the respective genes in the eyes of *Stra6*$^{-/-}$ and WT mice. We observed that the expression of the *Rho* mRNA was ~60% in 1-month-old and ~80% in 8-month-old *Stra6*$^{-/-}$ mice of age-matched WT mice (Fig. 3A and B). Additionally, we analyzed the expression of G protein subunit alpha transducin 1 (*Gnat1*) and transducin 2 (*Gnat2*), which are a rod- and cone-specific components of the phototransduction cascade (Supplementary Material, Fig. S1A–D). The expression of *Gnat1* followed a similar pattern as the expression of the *Rho* gene (Supplementary Material, Fig. S1A and B). Based on the immunostaining of the retinal sections, the density of Rho protein appeared to be lower in 1-month-old *Stra6*$^{-/-}$ mice than in age-matched WT mice. At 8 months of age, staining of Rho was comparable between *Stra6*$^{-/-}$ and WT mice (Fig. 3C-F).

The expression levels of *Opn1mw* and *Opn1sw* were lower in *Stra6*$^{-/-}$ mice than in WT mice at all ages examined. In 1-month-old *Stra6*$^{-/-}$ mice, mRNA levels of *Opn1sw* were ~20% (Fig. 3G) and *Opn1mw* were ~50% (Fig. 3M) of WT mice. The expression of *Gnat2* mRNA was also significantly lower at this age (Supplementary Material, Fig. S1C and D). The mRNA expression levels of the *Opn1sw* and *Opn1mw* cone opsins did not increase in 8-month-old mice (Fig. 3H and N). Accordingly, staining for S-opsin was barely detectable in retinal sections of both 1- and 8-month-old *Stra6*$^{-/-}$ mice, whereas staining for M-opsin was highly reduced or mislocalized in retinal cryosections of *Stra6*$^{-/-}$ mice. In contrast, age-matched WT mice displayed strong staining for the S- and M-opsin throughout the photoreceptor outer segment layer of the retina (Fig. 3I–L and O–R). To distinguish whether the reduced M and S-cone staining is related to impaired cone visual pigment maturation caused by chromophore deficiency or to cone photoreceptor cell death, we performed whole mount staining with peanut agglutinin (PNA). Staining with the cone plasma membrane marker revealed distinct patterns of cone photoreceptors in 2-, 5- and 7-month-old *Stra6*$^{-/-}$ mice (Supplementary Material, Fig. S2A–C). As a negative control, we performed staining for PNA in an *Lrat*$^{-/-}$;*Stra6*$^{-/-}$ double mutant (Supplementary Material, Fig. S2D). The *Lrat* genotype causes an entire lack of chromophore and cone photoreceptors degenerate under this condition (34). In conclusion, PNA staining indicated that cone photoreceptors apparently survived in *Stra6*$^{-/-}$ mice, whereas cone photoreceptors degenerated in an LRAT and STRA6-defcient double mutant.

Visual responses are highly reduced in *Stra6* $^{-/-}$ mice

We next recorded the electrical responses to light generated by rods in dark-adapted eyes, and the responses generated by cones

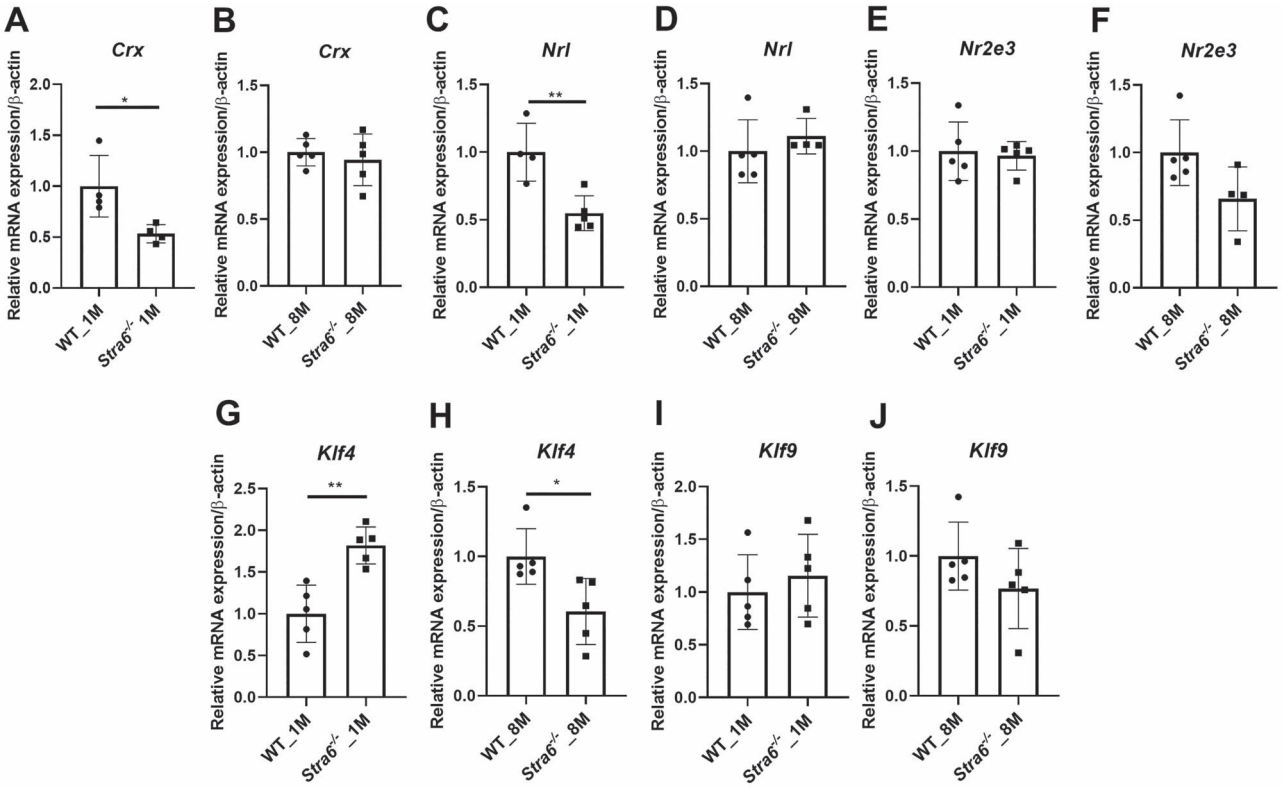

Figure 2. Expression of rod and cone transcription factors. **(A–F)** Quantitative RT-PCR analysis for the rod marker genes *Crx*, *Nrl and Nr2e3* in total RNA preparations of the retina in 1- and 8-month-old *Stra6*$^{-/-}$ mice and WT mice ($n = 5$ per genotype and age). **(G–J)** qRT-PCR analysis for cone marker genes *Klf4* and *Klf9* with total RNA preparations of the retina of 1- and 8-month-old *Stra6*$^{-/-}$ mice and WT mice ($n = 4$–5 per genotype and age). *β-Actin* gene expression was used as internal control. Values were normalized to the corresponding values of age-matched WT mice and are displayed as mean ± SD. $^{*}P < 0.05$; $^{**}P < 0.005$, $^{***}P < 0.0001$. The statistical analysis was performed using unpaired two-tailed Student's *t*-test by comparing values from age-matched *Stra6*$^{-/-}$ and WT mice.

in light-adapted eyes by electroretinography (ERG) (35,36) (Fig. 4). The analyses revealed that recorded scotopic ERG responses (a- and b-waves) to flash light stimuli were highly diminished in 1-month-old *Stra6*$^{-/-}$ mice in comparison with WT mice (Fig. 4A and B). The ERG responses significantly improved in 8-month-old *Stra6*$^{-/-}$ mice (Fig. 4C and D). However, a and b wave amplitudes did not reach values of WT mice.

We next determined the ERG responses in light-adapted mice of different ages. Under photopic conditions, ERG responses were barely detectable even at the highest illuminance in 1-month-old *Stra6*$^{-/-}$ mice when compared to WT mice (Fig. 4E). Notably, the photopic responses remained very low in 8-month-old *Stra6*$^{-/-}$ mice and mirrored the reduced S- and M-opsin expression in the retinas of the mice (Fig. 4F).

Photoreceptors of *Stra6* $^{-/-}$ mice display significant levels of non-liganded rhodopsin

Stra6$^{-/-}$ mice displayed reduced scotopic responses although the expression of *Rho* was seemingly adjusted to the reduced ocular retinoid levels (Fig. 3A and B). We speculated that this phenotype is caused by imbalances between chromophore and opsin. It is widely accepted that unliganded rod opsin activates the phototransduction cascade even in darkness (37). The constitutive activity of unliganded rod opsin is equivalent to that of background light and results in a concurrent reduction in phototransduction gain (38). Therefore, we determined the levels of unliganded opsin in photoreceptors of this mouse mutant. SDS-PAGE of immune-purified RHO showed that the opsin content of outer segments from 1-month-old STRA6-deficient mice was lower than in age-matched WT mice (Fig. 5A). We then performed UV-visible spectrophotometry with the isolated protein fractions and compared the theoretical 280/500 nm ratio with the experimental ratio of absorption. We observed a ∼50% decrease of rhodopsin in 1-month-old *Stra6*$^{-/-}$ mice when compared to age-matched WT mice (Fig. 5B). In 8-month-old *Stra6*$^{-/-}$ mice, rhodopsin content increased as indicated by the SDS-PAGE (Fig. 5C). Accordingly, the 280–500 nm ratio significantly shifted towards liganded rhodopsin (Fig. 5D). However, 9% of unliganded opsin were still present in the rhodopsin fraction isolated from dark-adapted photoreceptor outer segments (Fig. 5C and D). We also determined 11-*cis*-RAL levels in dark-adapted *Stra6*$^{-/-}$ and WT mice by HPLC analysis. One-month-old *Stra6*$^{-/-}$ mice displayed 20% and 8-month-old mice displayed 79% of the 11-*cis*-RAL concentration of aged-matched WT mice (Fig. 5E and F).

To provide additional evidence for the existence of unliganded opsin in photoreceptors, we supplemented dark-adapted *Stra6*$^{-/-}$ and WT mice with the chromophore surrogate 9-*cis*-RAL, which can occupy the chromophore binding pocket of unliganded rod and cone opsins. Upon supplementation, we detected significant amounts of 9-*cis*-RAL in HPLC analysis of the eyes of *Stra6*$^{-/-}$ but not in WT mice (Supplementary Material, Fig. S3A). In 1-month-old *Stra6*$^{-/-}$ mice, calculation of the molar amounts indicated that 9-*cis*-RAL constituted about 50% of the total chromophore concentration (Fig. 5G). The content of 9-*cis*-RAL was lower in 8-month-old *Stra6*$^{-/-}$ mice in the HPLC measurement

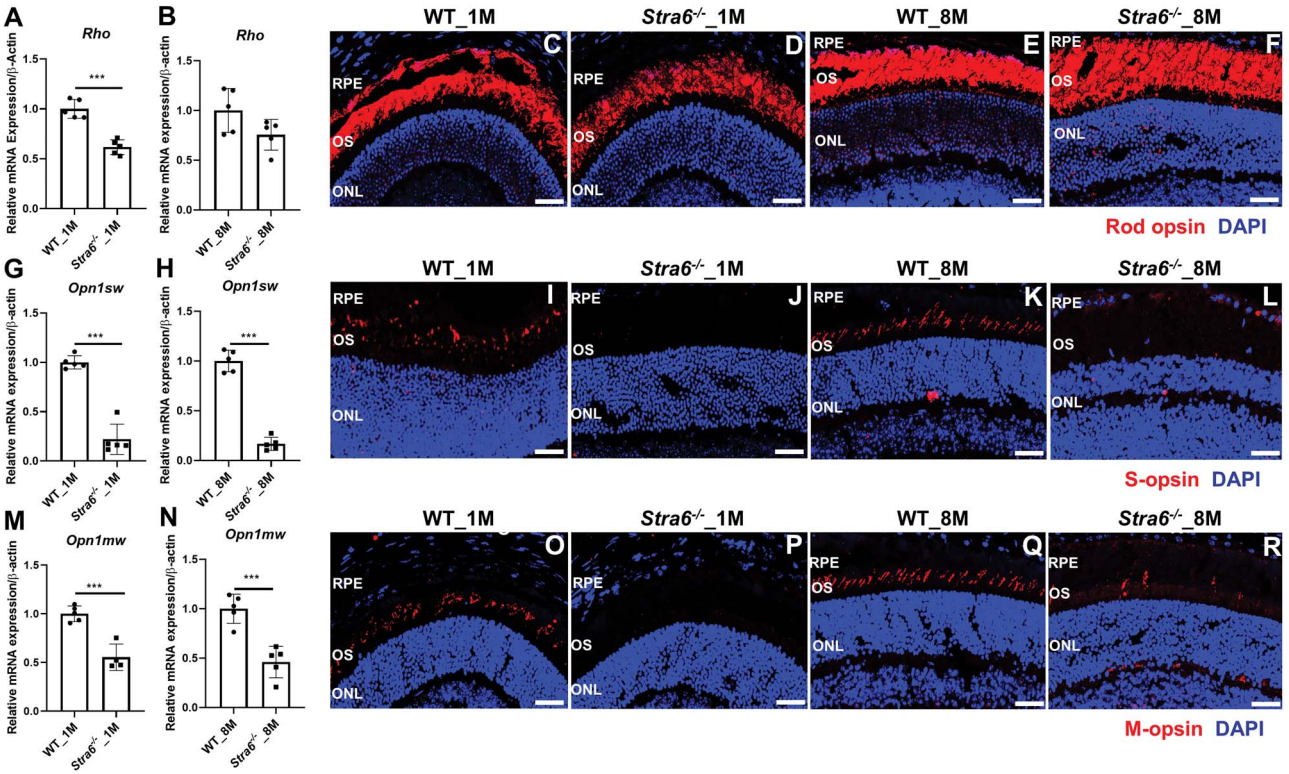

Figure 3. STRA6-deficient mice display reduced expression of cone and rod opsins. (**A**, **B**) Quantitative RT-PCR analysis for *Rho* in total RNA preparations of the retina in 1- and 8-month-old *Stra6*$^{-/-}$ mice and WT mice ($n = 5$ per genotype and age). (**C–F**) Immunohistochemistry of representative retinal cryosections stained for rod opsin. Nuclei are stained with DAPI. (**G**, **H**) Quantitative RT-PCR analysis for *Opn1sw* in total RNA preparations of the retina in 1- and 8-month-old *Stra6*$^{-/-}$ mice and WT mice ($n = 5$ per genotype and age). (**I–L**) Immunohistochemistry of representative retinal cryosections stained for S-opsin. Nuclei are stained with DAPI. (**M**, **N**) Quantitative RT-PCR analysis for *Opn1mw* in total RNA preparations of the retina in 1- and 8-month-old *Stra6*$^{-/-}$ mice and WT mice ($n = 5$ per genotype and age). (**O–R**) Immunohistochemistry of representative retinal cryosections stained for M-opsin. Nuclei are stained with DAPI. All the images were taken by confocal microcopy at 40× magnification and scale bar represents 50 μm. OS, outer segments and ONL, outer nuclear layer.

(Supplementary Material, Fig. S3B) albeit it still constituted 8% of total ocular chromophore concentration (Fig. 5H). Together, our analyses revealed that dark-adapted *Stra6*$^{-/-}$ mice displayed an imbalance between opsin and chromophore concentrations at all examined ages.

High dose vitamin A supplementation of mice

We next examined whether an intervention with pharmacological doses of vitamin A can rescue the visual phenotype of STRA6-deficient mice. We dark adapted mice for 12 h and administered the chromophore precursor in three consecutive intraperitoneal injections (1 mg ROL per mouse) in 1-day interval (Fig. 6A). During the intervention, mice were kept in darkness. To determine the effect of the treatment, we performed ERG analysis 2 days after the last treatment. In 1-month-old *Stra6*$^{-/-}$ mice, scotopic a and b wave amplitudes considerably increased in treated mice when compared to non-treated mice (Fig. 6B and C). In 8-month-old mice, we observed no significant improvement of the scotopic ERG responses after ROL intervention (Fig. 6D and E). We next analyzed the total ocular retinoid concentration in treated and control mice. HPLC analysis revealed that the 11-*cis*-RAL concentration doubled in 1-month-old *Stra6*$^{-/-}$ mice after treatment with ROL. In 8-month-old mice, a slight increase of 11-*cis*-RAL was observed which did not reach significance in statistical analysis. The same slight increase in 11-*cis*-RAL was observed in ROL-treated WT mice (Fig. 6F and G). However, treated WT mice also displayed a 5-fold increase in ocular RE levels and accumulated up to 600 pmol of REs per eye, whereas *Stra6*$^{-/-}$ mice displayed only a marginal increase in REs (Fig. 6H and I). Spectroscopic analysis of isolated rhodopsin showed that untreated 1- and 8-month-old *Stra6*$^{-/-}$ mice displayed unliganded rod opsin even upon prolonged dark adaption (Fig. 7A and B). Treatment with ROL increased the content of rhodopsin in 1-month-old *Stra6*$^{-/-}$ mice (Fig. 7C and D) but no increase was observed in 8-month-old mice (Fig. 7E and F). Thus, ROL treatment improved rod photoreceptor function in 1-month-old but not 8-month-old *Stra6*$^{-/-}$ mice.

We also analyzed cone photoreceptor function in ROL-treated mice. In ERG analysis, photopic responses remained unchanged in treated when compared to untreated *Stra6*$^{-/-}$ mice (Fig. 6J and K). Accordingly, immunostaining of retinal cryosection revealed absent and/or mislocalized staining for M-opsin (Fig. S4), indicating that pharmacological doses of ROL did not rescue cone visual pigment biogenesis in STRA6-deficient mice.

STRA6 deficiency leads to retinal degeneration

Chromophore deficiency can trigger retinal pathologies and is associated with retinal degenerative phenotypes such Leber congenital amaurosis (37,39) and retinitis pigmentosa (40,41). However, it is not fully understood if the depletion of STRA6 would lead to retinal degeneration. Thus, we examined retinal morphology of *Stra6*$^{-/-}$ mice using optical coherence tomography (OCT), scanning laser ophthalmoscopy (SLO), histological analyses and morphometry (Fig. 8A–P). SLO analyses of 8-month-old

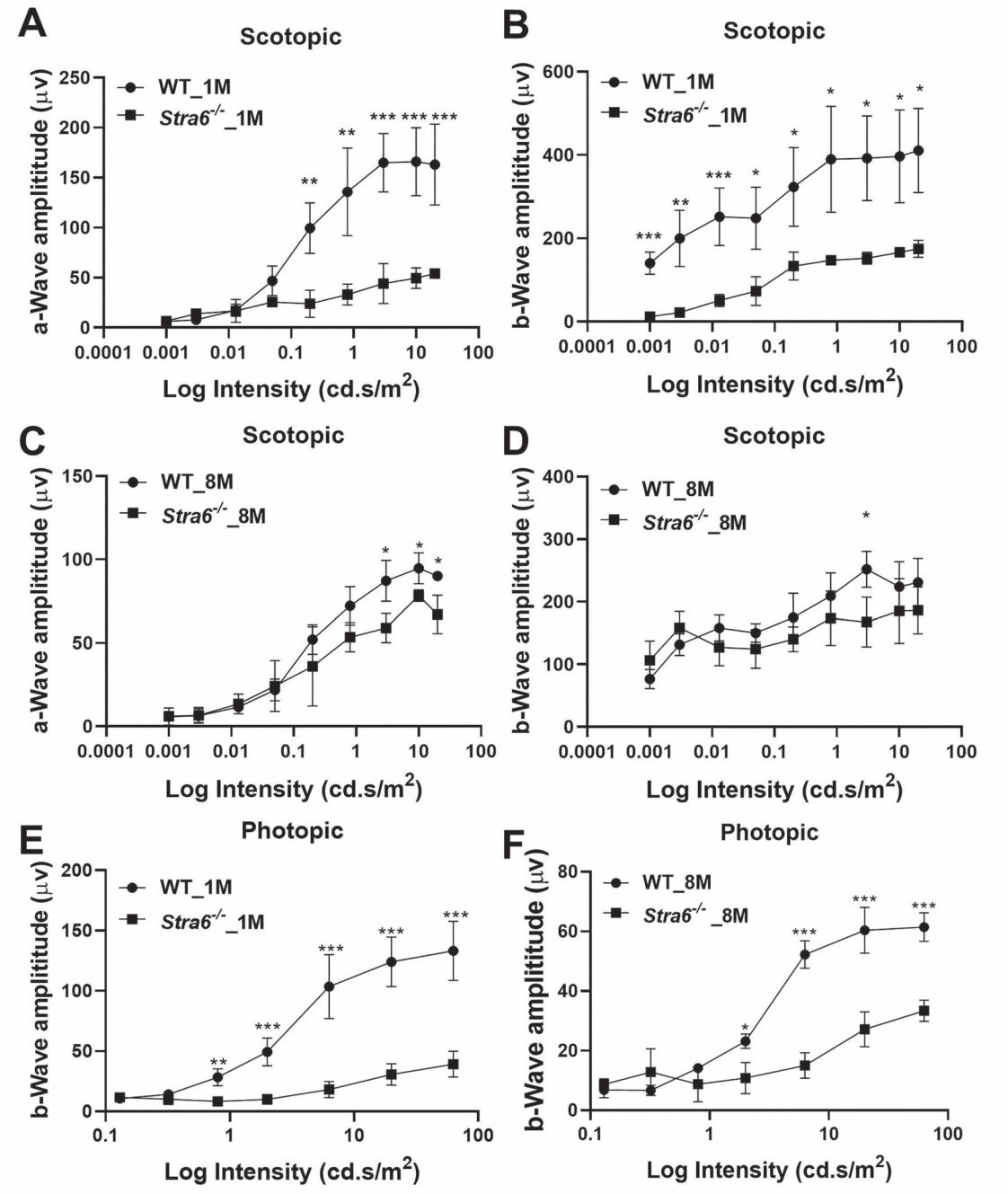

Figure 4. ERG responses of STRA6-deficinet mice at different ages. ERG responses were recoded from 1- and 8-month-old *Stra6*$^{-/-}$ and age-matched WT mice ($n = 3$ per age and genotype) (**A**, **B**) a- and b-wave amplitudes under scotopic conditions from 1-month-old mice. (**C**, **D**) a- and b-wave amplitudes under scotopic conditions from 8-month-old mice. (**E**, **F**) b-wave amplitudes under photopic conditions from 1- and 8-month-old *Stra6*$^{-/-}$ and WT mice. Statistical analyses were performed by comparing age-matched mice of both genotypes using unpaired two-tailed Student's *t*-test. *$P < 0.05$; **$P < 0.005$, ***$P < 0.0001$. The statistical analysis was performed using unpaired two-tailed Student's *t*-test by comparing values from age-matched *Stra6*$^{-/-}$ and WT mice.

Stra6$^{-/-}$ mice revealed bright fluorescent spots in the ventral retina that were not observed in age-matched WT control mice (Fig. 8D and P). These spots are characteristic for the activation of microglia and macrophages that migrate to the retina to clear dying retinal cells (42,43). The OCT analysis revealed that 1-month-old *Stra6*$^{-/-}$ mice displayed similar outer nuclear layer (ONL) thickness as WT control mice (Fig. 8 E and F). In 8-month-old *Stra6*$^{-/-}$ mice, we observed a significant reduction in ONL thickness when compared to age-matched WT controls (Fig. 8G and H). The retina ONL thickness measured by OCT and averaged thickness of the retina ONL of 1- and 8-month-old *Stra6*$^{-/-}$ mice were plotted in the graph. This analysis confirmed that there was a considerable difference between 8-month-old *Stra6*$^{-/-}$ and WT mice. (Fig. 8M and N). The outcome of the OCT analyses was confirmed by retinal histology that revealed a significant difference in the number of nuclei in the ONL of 8-month-old *Stra6*$^{-/-}$ mice when compared to age-matched WT mice (Fig. 8O).

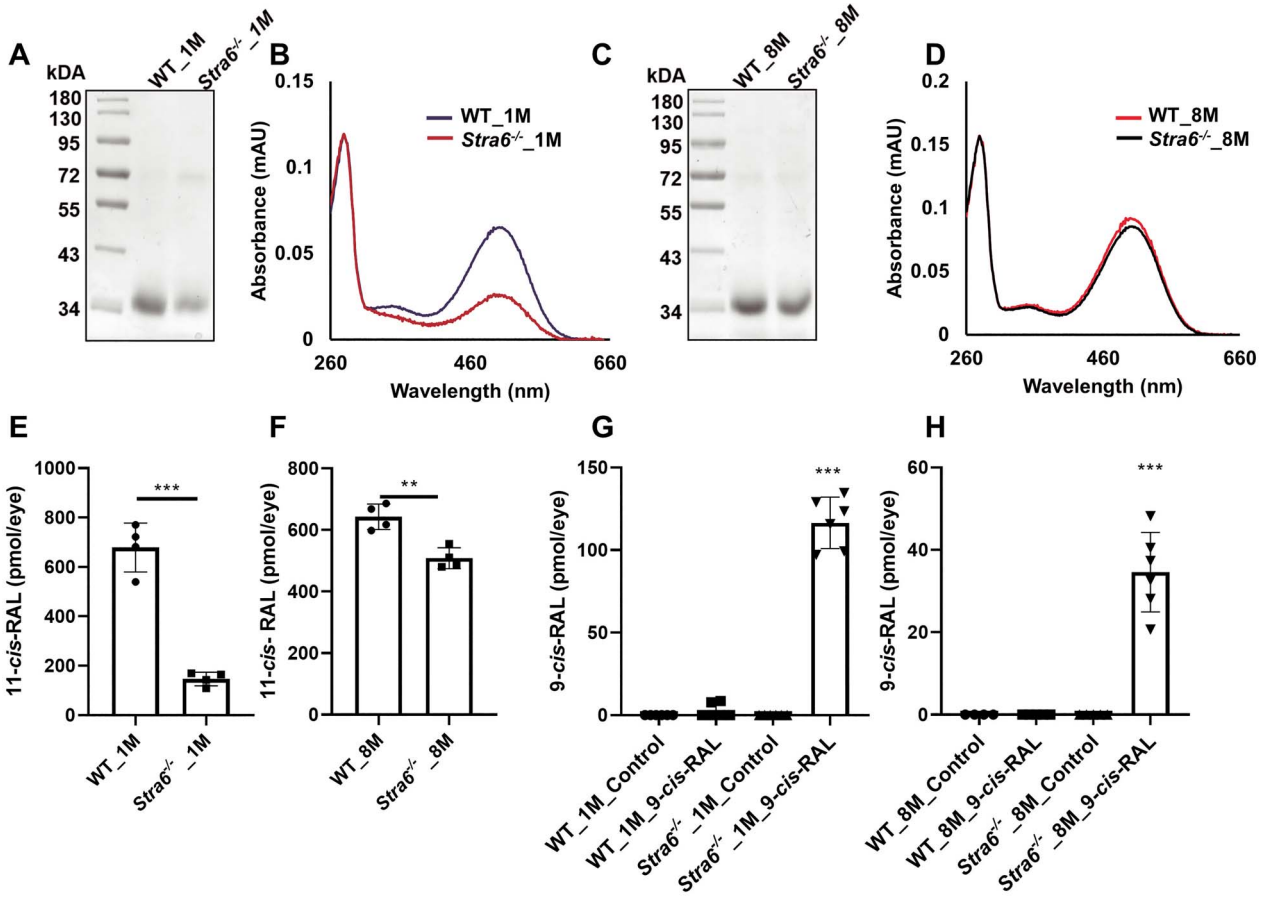

Figure 5. Unliganded rod opsin in photoreceptors of *Stra6*$^{-/-}$ mice. (**A**) Representative SDS-PAGE of the 1D4 immune-purified rhodopsin fraction of 1-month-old *Stra6*$^{-/-}$ and WT mice. (**B**) UV-visible spectra of the immune-purified rhodopsin fractions for 1-month-old mice. (**C**) Representative SDS-PAGE of the 1D4 immune-purified rhodopsin fraction of 8-month-old *Stra6*$^{-/-}$ and WT mice. (**D**) UV-visible spectra of the immune-purified rhodopsin fractions for 8-month-old mice. (**E**) 11-*cis*-RAL content of 1-month (**F**) and 8-month-old *Stra6*$^{-/-}$ and WT mice. (**G**) 9-*cis*-RAL content of 1-month (**H**) and 8-month-old *Stra6*$^{-/-}$ and WT mice upon 9-*cis*-RAL supplementation. Statistical analyses were performed by comparing age matched mice of both genotypes using unpaired two-tailed Student's *t*-test. $^{**}P < 0.005$, $^{***}P < 0.0001$.

Discussion

Initial studies in knockout mice led to the proposal that the lipoprotein, as well as the RBP and STRA6-dependent pathways for vitamin A delivery, is complementary and that only when all delivery pathways fail peripheral tissues will suffer from vitamin A deficiency (7). We here scrutinized the role of STRA6 in ocular vitamin A uptake homeostasis in mice. We observed that STRA6 is critical for photoreceptor maintenance and functioning and that the mouse eyes display characteristic features of ocular vitamin A deprivation in the absence of the vitamin A transporter at all ages. The implications of these findings for ocular vitamin A homeostasis in health and disease are discussed below.

Vitamin A deficiency is a major public health problem in developing countries, adversely affecting vision of millions of children and pregnant women (44,45). Seminal work by Dowling and Wald described the ocular consequences of vitamin A deprivation in the rat model (46). The depletion of liver stores in these rats was followed by a decrease in blood vitamin A levels. In the eyes, rhodopsin declined first before the chromophore-free opsin vanished (46). Because dietary vitamin A deprivation is difficult to achieve in rodents, mouse mutants with impaired chromophore synthesis were later used to study the consequences of ocular vitamin A deficiency (47). It was shown in these mutant mice that unliganded rod opsin activates sensory transduction in the dark and triggers a slow degeneration of rod photoreceptors (37,39). Additionally, these mice suffer from early cone photoreceptor degeneration (48). In the absence of the chromophore, cone opsins and other components of the signaling transduction cascade are not trafficked to the outer segments of cone photoreceptors (49). We here demonstrated that the STRA6 protein is critical to prevent such phenotypes of photoreceptors. In its absence, mice displayed similar characteristics as have been reported for chromophore-deficient photoreceptors. These included increased levels of unliganded rod opsin and absent or mislocalized cone opsins. Though the ocular retinoid content increased during adolescence, significant amounts unliganded rod opsin persisted in the retina and cone photoreceptors remained chromophore deficient. The cone phenotype indicated that rods entrap the available chromophore in the STRA6-deficient retina and cones were poorly supplied with this retinoid. Such competition between rod and cone photoreceptors for chromophore has been previously convincingly demonstrated in the *Rpe65* R91W mutant mice (50). We can exclude that the cone phenotype of *Stra6*$^{-/-}$ mice was caused by photoreceptor cell death. The retina of 8-month-old *Stra6*$^{-/-}$ mice still expressed cone-specific marker genes and cones staining with PNA observed cones at all ages of *Stra6*$^{-/-}$ mice.

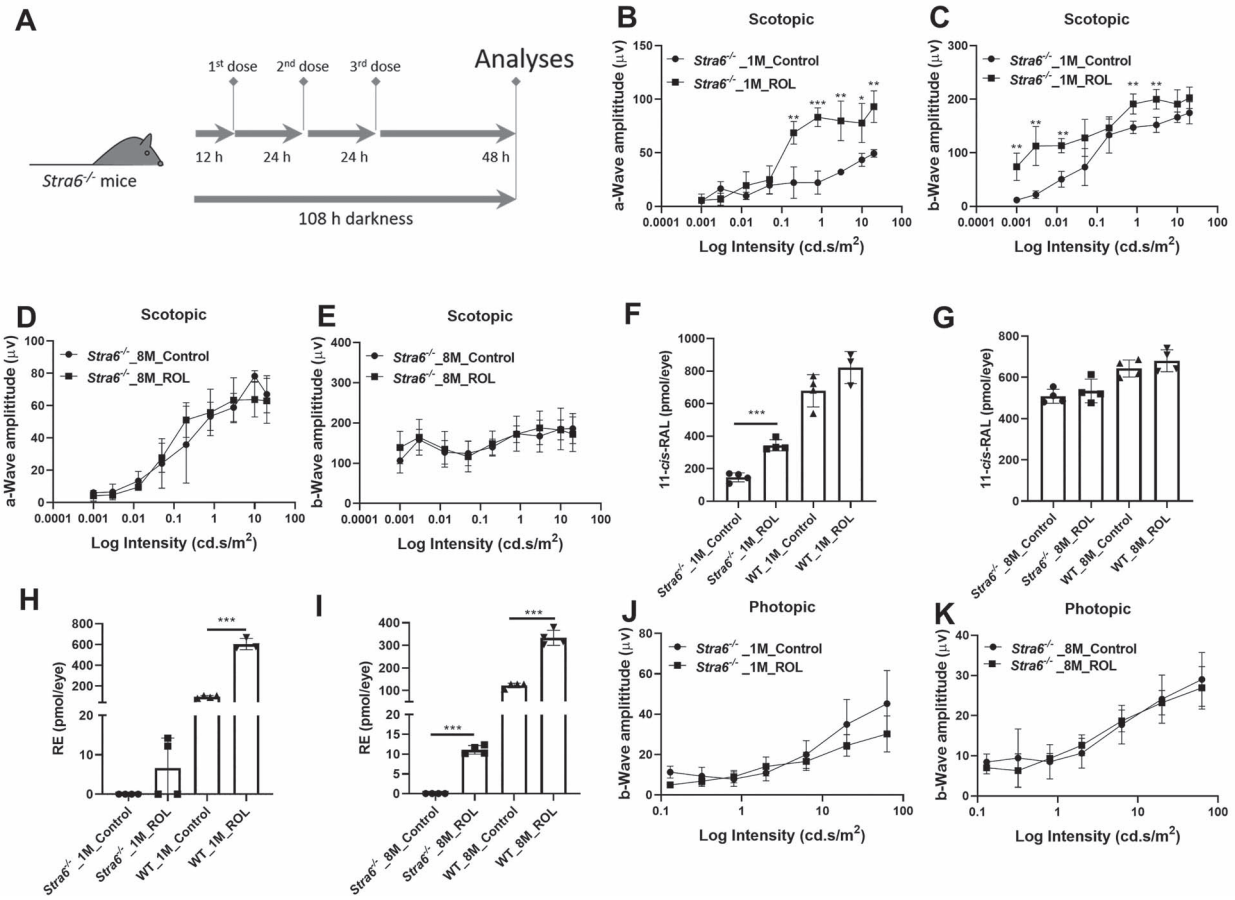

Figure 6. Pharmacological doses of retinol do not rescue the photoreceptor phenotype of *Stra6*$^{-/-}$ mice. (**A**) Scheme of the rescue experiment. One- and 8-month-old *Stra6*$^{-/-}$ mice were injected with three consecutive doses of ROL (1 mg per injection). Untreated control mice were constantly kept in darkness. (**B**, **C**) a- and b-wave amplitudes under scotopic conditions from 1-month-old treated and untreated *Stra6*$^{-/-}$ mice. (**D**, **E**) a- and b-wave amplitudes under scotopic conditions from 8-month-old treated and untreated *Stra6*$^{-/-}$ mice. (**F**, **G**) 11-cis-RAL concentration of 1-month-old ROL treated and untreated *Stra6*$^{-/-}$ and WT mice and (**G**) 8-month-old ROL treated and untreated *Stra6*$^{-/-}$ and WT mice. (**H**, **I**) RE concentration of 1-month-old ROL treated and untreated *Stra6*$^{-/-}$ and WT mice and (**I**) 8-month-old ROL treated and untreated *Stra6*$^{-/-}$ and WT mice. (**J**, **K**) b-wave amplitudes under photopic conditions from 1- and 8-month-old treated and untreated *Stra6*$^{-/-}$ mice. $^{*}P < 0.05$; $^{**}P < 0.005$, $^{***}P < 0.0001$. Statistical analyses were performed by comparing age matched mice of both genotypes using unpaired two-tailed Student's *t*-test.

However, the cones did not synthesize cone visual pigments because chromophore supply was disrupted in the absence of STRA6. The analysis of rod photoreceptors indicated that STRA6 is essential to maintain the stoichiometry of opsins and chromophore. Fifty percent of rod pigment was ligand-free at 1 month of age. The opsin-chromophore imbalance was still observed in 8-month-old *Stra6*$^{-/-}$ mice, indicating that STRA6 is critical to balance ocular retinoid levels and adjust it to the opsin levels throughout the life cycle. STRA6 deficiency also had affected the expression of cone- and rod-specific markers, including cone and rod opsins and their respective G proteins, essential components of the phototransduction cascade. Despite this adjustment, the stoichiometry between opsin and chromophore could not be established in the retinas of STRA6-deficient mice. This imbalance was associated with a retinal degeneration phenotype associated with an accumulation of fluorescent speckles and the outer segment thinning when *Stra6*$^{-/-}$ mice aged.

Remarkably, the imbalance between opsins and chromophore could not been corrected by intervention with pharmacological doses of vitamin A. Ocular retinoid levels of *Stra6*$^{-/-}$ mice only slightly increased upon this treatment, whereas the eyes of WT mice showed a substantial increase of retinoids (mainly REs) upon treatment with three consecutive doses of vitamin A. Previously, a strongly diminished ocular retinoid uptake has been reported in RBP and LRAT-deficient mice (21,51). LRAT works downstream of STRA6 and esterifies ROL into REs (16,21). We observed highly reduced ocular concentration of REs in *Stra6*$^{-/-}$ mice. The same biochemical phenotype was reported in mice that lack the STRA6 ligand, RBP (9). Based on these findings, we propose that STRA6 is required to accumulate enough retinoids in the eyes to build an ocular RE pool. We propose that the ocular RE pool must exceed the available binding sites for chromophore in the opsin moieties of visual pigments in rod and cone photoreceptors. The build-up of the RE pool is critical to sustain chromophore synthesis as needed for visual pigment synthesis and recycling. In STRA6-deficient mice, the ocular RE pool cannot be established, and therefore, the stoichiometry of chromophore and opsins is disrupted. The study also sheds new light on RE storing lipid droplets, so-called retinosomes (52), and indicate that these lipid structures are critical for chromophore homeostasis of the eyes.

It needs to be clarified how STRA6 and LRAT interact in the synthesis of REs and how this pathway is regulated. Recent structural analysis revealed that STRA6 binds calmodulin (53) and that calcium signaling affects the direction of vitamin A

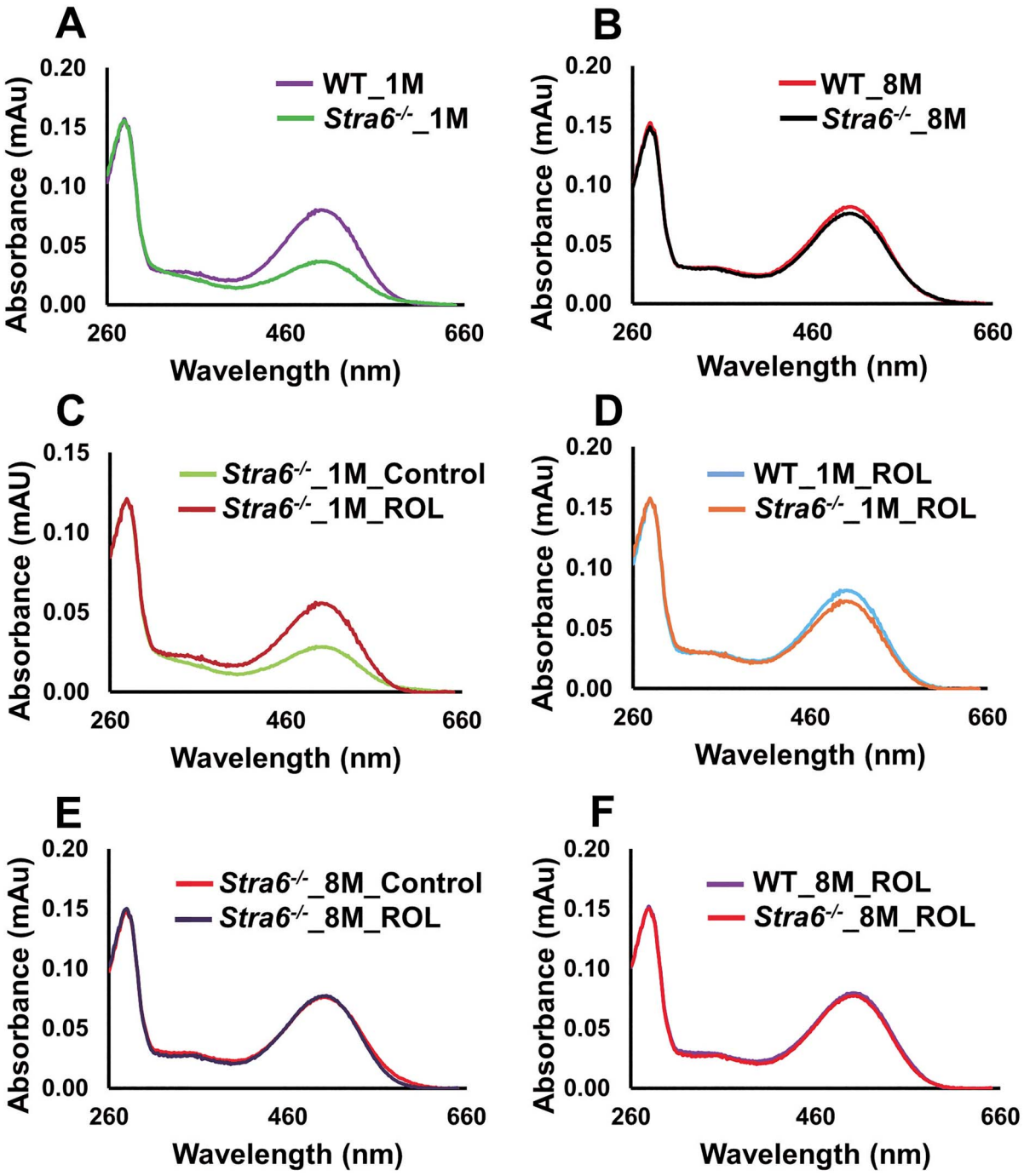

Figure 7. Ratio of unliganded versus liganded rod opsin in vitamin A treated *Stra6*$^{-/-}$ mice. (**A–C**) Comparison of the UV-visible spectra of the immune-purified rhodopsin fractions of (A) 1-month-old *Stra6*$^{-/-}$ and WT mice, (B) 8-month-old *Stra6*$^{-/-}$ and WT mice, (C) 1-month-old treated and untreated *Stra6*$^{-/-}$ mice, (**D**) 1-month-old ROL-treated *Stra6*$^{-/-}$ and WT mice, (**E**) 8-month-old treated and untreated *Stra6*$^{-/-}$ mice, (**F**) 8-month-old ROL-treated *Stra6*$^{-/-}$ and WT mice.

transport (27). Interestingly, the expression levels of the retinoid isomerase RPE65 are controlled by ERK1/2 (54). RPE65 converts RE into 11-*cis*-retinol in chromophore synthesis and recycling (55,56). Thus, emerging evidence indicate an interplay between calcium signaling and ocular retinoid metabolism. Knowledge about the molecular basis of the mechanism that controls ocular vitamin A uptake homeostasis and chromophore synthesis will help to establish therapies to fight blinding diseases.

Materials and Methods

Animals, husbandry and diets

The generation of *Stra6*$^{-/-}$ mice has been previously described (24). WT mice were purchased from Jackson Laboratory. All mice were on a C57BL/6J genetic background and were bred and raised on regular chow diet (Prolab RMH 5000, vitamin A content 15 000 IU/kg diet). Mice had ad libitum access to food and water

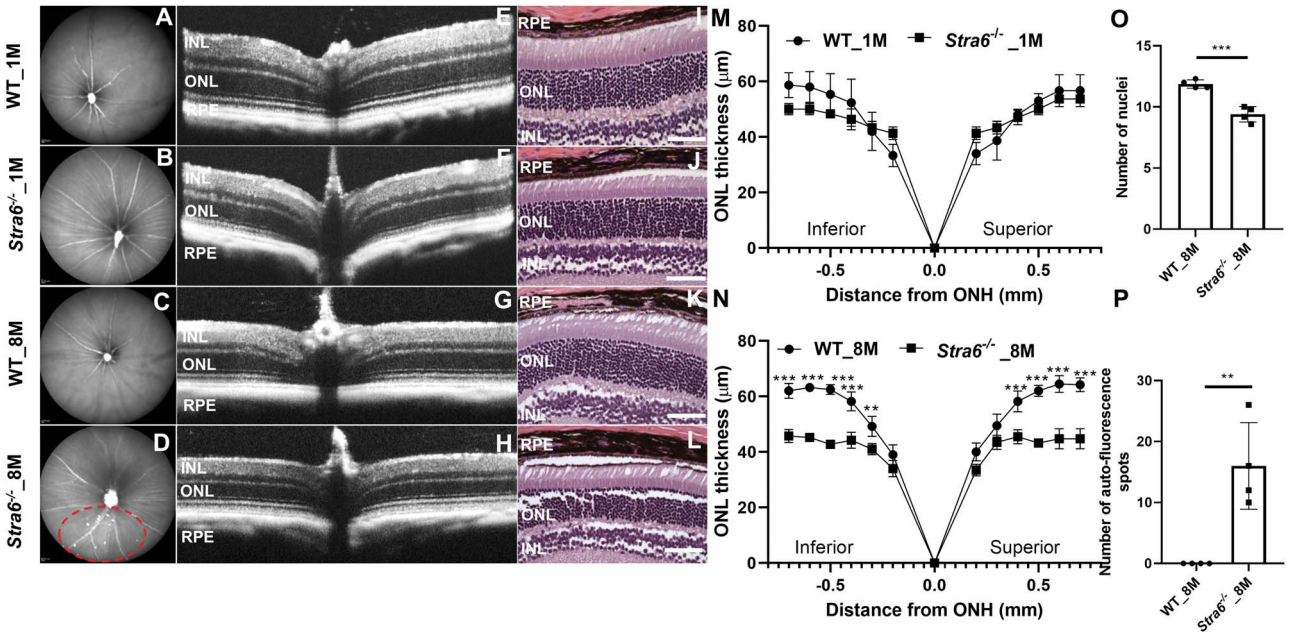

Figure 8. STRA6-deficient mice display a degenerative retina phenotype. (**A–D**) Representative fundus images (left panel), OCT images (middle panel) and H&E-stained histological images of the retina of (A, B) Fundus image for 1-month-old WT mouse and *Stra6*$^{-/-}$, (C, D) Fundus image for 8-month-old WT mouse and *Stra6*$^{-/-}$. The red dashed circle indicates a fundus region with pronounced autofluorescent spots. (**E, F**) Representative OCT image for 1-month-old WT and *Stra6*$^{-/-}$ mice. (**G, H**) Representative OCT image for 8-month-old WT mouse and *Stra6*$^{-/-}$. (**I, J**) Histology images for 1-month-old WT mouse and *Stra6*$^{-/-}$. (**K, L**) Histology images for 8-month-old WT and *Stra6*$^{-/-}$ mice. (**M, N**) The retina ONL thickness of the retina ($n = 4$) from each group were measured by OCT. The averaged thickness of the retina ONL was blotted as graph for (M) 1-month and (N) 8-month-old WT and *Stra6*$^{-/-}$ mice. (**O**) Counts of the number of nuclei in the ONL of 8-month-old *Stra6*$^{-/-}$ and WT mice ($n = 4$ per genotype and age). (**P**) Number of autofluorescent spots in SLO fundus images of 8-month-old *Stra6*$^{-/-}$ and WT mice ($n = 4$ per genotype). $^{*}P < 0.05$; $^{**}P < 0.005$, $^{***}P < 0.0001$. The statistical analysis was performed using unpaired two-tailed Student's *t*-test by comparing age-matched WT mice as control. ONH, optic nerve head.

at 24°C in a light–dark cycle. We use female mice for all our experiment to avoid gender variations. All animal procedures and experiments were approved by the Case Western Reserve University Animal Care Committee (Protocol # 2014-0106) and ARVO Statement for the Use of Animals in Ophthalmic and Vision Research.

Immunofluorescence

Eyes from 1- and 8-month-old WT and *Stra6*$^{-/-}$ mice were dissected and immediately fixed overnight in 4% paraformaldehyde (Electron Microscopy Sciences, Hatfield, PA). Visual Sciences Research Center core facility at Case Western Reserve University was procured for preparation of tissue blocks and sectioning. The 10 μm eye sections were blocked with 5% goat serum in PBS-T (PBS with 0.1% Triton X-100) for 2 h at room temperature and then incubated with either M-cone (Catalog number AB5405, Millipore Sigma, St. Louis, MO) or S-cone antibody (Catalog number ABN1660, Millipore Sigma) prepared in blocking buffer overnight at 4°C. For rhodopsin staining, the sections were incubated monoclonal 1D4 anti-rhodopsin antibodies (from R. Molday, University of British Columbia, Canada), followed by three 15 min washes with PBS-T. Slides were then incubated with goat anti-rabbit Alexa Fluro 555 secondary antibody for cone opsins and anti-mouse Alexa Fluro 555 secondary antibody (Invitrogen, Carlsbad, CA, USA) for rhodopsin in blocking buffer for 2 h. Sections were washed three times for 15 min with PBS-T and counterstained with DAPI-fluoromount G (Southern Biotech, Birmingham, AL) and mounted for confocal microscopy. All images were taken with a 40×/1.3NA oil immersion objective. The resolution of the images of the retina was obtained by 2048 pixels wide by 2048 pixels high with a scale of 142 nm per pixel using a Leica TCS SP8 with HyVolution2 confocal microscope.

Analysis of retinoids

For ocular retinoid extraction, *Stra6*$^{-/-}$ and WT mice were euthanized by rodent cocktail (20 mg/ml ketamine+1.75 mg/ml xylazine). Eyes ($n = 4$ per genotype and age) were dissected for retinoid extraction. To each eye, 200 μl of 2 M Hydroxylamine (pH 6.8) was added. The eyes were homogenized in a glass potter and sonicated for 30 s under dim red safety light (600 nm). Retinoids were extracted twice with the mixture containing 200 μl methanol, 400 μl acetone and 500 μl hexanes. HPLC analysis was performed on a normal-phase Zorbax Sil (5 μm, 4.6 × 150 mm) column. HPLC separation was achieved by isocratic flow of 90% hexanes with 10% ethyl acetate. HPLC was previously scaled with synthesized standards for quantification of molar amounts of retinoids (57).

SD-OCT and fundus imaging

Pupils of *Stra6*$^{-/-}$ and WT mice were fully dilated with 1% tropicamide (Bausch and Lomb, Tampa, FL) and mice were anesthetized by intraperitoneal injection of rodent anesthetic cocktail (20 mg/ml ketamine and 1.75 mg/ml xylazine). Mice whiskers were trimmed to avoid artifacts. Spectral domain optical coherence tomography (SD-OCT) images were acquired in the linear B-scan mode of an ultra-high-resolution SD-OCT instrument (Bioptigen, Morrisville, NC). Confocal scanning laser ophthalmoscope (SLO; Spectralis HRA2; Heidelberg Engineering, Heidelberg, Germany) was performed with a 55-degree lens to collect mouse fundus images. The near infrared (IR) reflectance image (IR mode, 820 nm laser) was used to align the fundus camera relative to the pupil to obtain an evenly illuminated fundus image. ONL thickness was calculated using software of the SD-OCT instrument. The thickness of the ONL was measured from

0.2 mm distance from the optic nerve head and measurements were reported at every 0.1 mm intervals.

Histology

Histological analyses were conducted by the Visual Sciences Research Center Core at Case Western Reserve University. The eyes of WT and *Stra6*$^{-/-}$ mice were fixed in 4% paraformaldehyde overnight and embedded in paraffin blocks. 10 μm slices were mounted on the glass slides for hematoxylin and eosin staining.

Purification of rhodopsin

Eyes were collected from dark-adapted *Stra6*$^{-/-}$ and WT mice at different ages. Eyes were either stored at −80°C or used immediately. Rhodopsin was purified as described previously (58). Eyes were homogenized gently with a glass–glass homogenizer in the buffer consisting of 20 mM *bis*-tris propane (BTP) (pH 7.5), 150 mM NaCl, 1 mM EDTA and protease inhibitor cocktail in the dark. The homogenates were centrifuged for 15 min at 16 000*g* in a benchtop Eppendorf centrifuge at 4°C. Supernatants were discarded, and pellets were solubilized in 20 mM BTP (pH 7.5), 100 mM NaCl, 20 mM n-dodecyl-β-D-maltoside (DDM) and protease inhibitor cocktail for 1 h at 4°C on a rotating platform. The membrane lysates were centrifuged at 16 000*g* for 60 min at 4°C. The resulting supernatants were mixed with 1D4-immunoaffinity resin (6 mg of 1D4 anti-rhodopsin antibody/ml resin) equilibrated with 20 mM BTP (pH 7.5), 100 mM NaCl and 2 mM DDM and incubated for 1 h at 4°C on a rotating platform. Then, the resin-supernatant mixture was transferred to the column, flow through was collected and the resin was washed with 20 mM BTP (pH 7.5), 500 mM NaCl and 2 mM DDM. Rhodopsin was eluted with 20 mM BTP (pH 7.5), 100 mM NaCl, 2 mM DDM supplemented by addition of 1D4 peptide (TETSQVAPA) at a final concentration of 0.1 mg $\times$ ml^{-1}. The UV-visible spectra of the eluted proteins were measured with a UV-visible Cary 60 spectrophotometer. The concentration of rhodopsin was calculated using the extinction coefficient $\varepsilon_{500} = 40\,600$ M^{-1} cm^{-1} (59,60). The concentration of ligand-free opsin was calculated using the extinction coefficient $\varepsilon_{280} = 81\,200$ M^{-1} cm^{-1}.

Electroretinography

Overnight dark-adapted 1- and 8-month-old WT and *Stra6*$^{-/-}$mice were anesthetized by rodent anesthetic cocktail (20 mg $\times$ ml^{-1} ketamine and 1.75 mg $\times$ ml^{-1} xylazine), and the pupils were dilated with 1% tropicamide (Bausch and Lomb, Tampa, FL). Mice were placed on a temperature-regulated heating pad throughout each recording session. Diagnosys Celeris rodent ERG device (Diagnosys, Lowell, MA) with an Ag-AgCL cornea electrode was used for recordings. Scotopic responses were obtained in the dark with 10 steps of white light, flash stimulus, ranging from 0.001 to 20 cd s $\times$ m^{-2}. The duration of the inter-stimulus intervals increased from 4 s for low-luminance flashes to 90 s for the highest stimuli. After 7 min of light adaptation, cone ERGs were recorded with strobe-flash stimuli (0.32 to 63 cd s $\times$ m^{-2}) superimposed on the adapting field.

Pharmacological rescue experiment with retinoids

One- and 8-month-old *Stra6*$^{-/-}$ and WT mice ($n = 5$ per genotype) were injected intraperitoneally with 1 mg/per mouse of ROL (Toronto Research Chemicals, Canada) dissolved in DMSO for consecutive 3 days. Three mice were euthanized 48 h post treatment and eyes ($n = 6$) were harvested for rhodopsin purification as described. The remaining mice were used to determine retinoid content and composition by HPLC analysis. In addition, 1- and 8-month-old *Stra6*$^{-/-}$ and WT mice ($n = 3$ per genotype and age) were dark adapted for 16 h and then injected intraperitoneally with 0.5 mg per mouse of 9-*cis*-RAL (Cayman Chemicals, Ann Arbor, MI) for three consecutive days. Mice were euthanized 24 h post treatment, eyes were dissected and ocular retinoid concentrations and composition were determined by HPLC.

qRT-PCR analysis of marker genes

Stra6$^{-/-}$ and WT mice ($n = 5$) were sacrificed and retinas were dissected. Total RNA was extracted from the retina by TRIZOL method (Invitrogen, Carlsbad, CA) and quantified using Nano drop ND-1000 spectrophotometer (Thermo Fisher Scientific, Waltham, MA). cDNA was generated using the High Capacity RNA to cDNA kit (Applied Biosystems, Thermo Fisher Scientific, Waltham, MA). Gene expression measurement was carried out by real-time quantitative PCR using an Applied Biosystems Real Time PCR instrument with Taq Man probes (Applied Biosystems; Thermo Fisher Scientific, Waltham, MA). Primers were *β-actin* (Mm02619580), *Gnat1* (Mm01229120), *Gnat2* (Mm00492394), *Rho* (Mm01184405), *Opn1mw* (Mm00433560), *Opnsw* (Mm00432058), *Crx* (Mm00483995), *Klf4* (Mm00516104), *Klf9* (Mm00495172), *Nr2e3* (Mm00443299) and *Nrl* (Mm00476550). Amplification was carried out using TaqMan polymerase. Fast Universal PCR Master Mix (2$\times$) No Amp Erase, UNG (Applied Biosystems; Thermo Fisher Scientific, Waltham, MA) following the manufacturer's protocol. 10 ng cDNA was used per 10 μl reaction. Gene expression levels were normalized to the expression of housekeeping gene β-actin using the $\Delta\Delta$Ct method. Statistical significance was calculated using unpaired two-tailed *t*-test using GraphPad Prism 8.0.

Immunohistochemistry and microscopy of retinal whole mounts

Mice were euthanized and the eyes were dissected and fixed in 4% paraformaldehyde in PBS for 1 h. The inferior side of the eyes was marked. The cornea was removed following the orientation of the *ora serrata*, and the lens and vitreous were removed from each eye cup. Radial incisions on eye cup were made to further flatten the retina. Retinas were washed two times in PBS containing 0.1% Triton X-100 (PBST). Cold methanol was dropped on retina drop by drop until flooded to further facilitate permeabilization. Retinas were further fixed and flattened in 4% paraformaldehyde between two coverslips for 30 min. Retinas were incubated over night at 4°C in anti-PNA antibody (Vector Laboratories, Burlingame, CA, catalog number B-1075-5) in PBST containing 4% goat serum. After incubation with primary antibodies, retinas were washed three times for 10 min in PBST and then incubated for 2 h at room temperature with secondary antibodies (Streptavidin, Alexa Fluor™ 488 conjugate, Invitrogen, Carlsbad, CA). Retinas were washed again two times for 10 min with PBST and then once with PBS. Finally, retinas were placed on microscope slides with photoreceptor side facing up, mounted with Vectashield mounting medium containing 4′,6-diamidino-2-phenylindol (catalog number H-1200; Vector Laboratories, Burlingame, CA) and protected with coverslips. Retinal whole mounts were imaged with a fluorescent microscope (Leica DMI6000B; Leica Microsystems Inc.) equipped with an automated stage. The microscope was set to scan the whole sample with a 10$\times$ objective. Individual images were stitched together automatically with MetaMorph 7.8 software (Molecular Devices, Sunnyvale, CA) to form panorama retinal images. The total cone counts were counted using MetaMorph software.

Statistical analysis

Data are displayed as the mean ± SD. Statistical analyses were performed using unpaired two tailed *t*-test and one-way ANOVA using Graph pad Prism 8.0 software and results were considered significant at $^{*}P < 0.05$, $^{**}P < 0.005$, $^{***}P < 0.0001$.

Supplementary Material

Supplementary Material is available at *HMG* online.

Acknowledgements

We thank Richard Lee for expert help with confocal microscopy and imaging and acknowledge the use of the Leica SP8 confocal microscope in the Light Microscopy Imaging Core at Case Western Reserve University made available through the Office of Research Infrastructure (National Institute of Health-ORIP) shared instrumentation grant S10OD024996.

Conflict of Interest statement. The authors declare that they have no conflicts of interest with the contents of this article.

Funding

National Eye Institute (EY028121 and EY011373).

References

1. von Lintig, J., Moon, J. and Babino, D. (2021) Molecular components affecting ocular carotenoid and retinoid homeostasis. *Prog. Retin. Eye Res.*, **80**, 100864.
2. D'Ambrosio, D.N., Clugston, R.D. and Blaner, W.S. (2011) Vitamin a metabolism: an update. *Nutrients*, **3**, 63–103.
3. von Lintig, J., Moon, J., Lee, J. and Ramkumar, S. (2020) Carotenoid metabolism at the intestinal barrier. *Biochim. Biophys. Acta Mol. Cell Biol. Lipids*, **1865**, 158580.
4. Batten, M.L., Imanishi, Y., Maeda, T., Tu, D.C., Moise, A.R., Bronson, D., Possin, D., Van Gelder, R.N., Baehr, W. and Palczewski, K. (2004) Lecithin-retinol acyltransferase is essential for accumulation of all-trans-retinyl esters in the eye and in the liver. *J. Biol. Chem.*, **279**, 10422–10432.
5. Goodman, D.W., Huang, H.S. and Shiratori, T. (1965) Tissue distribution and metabolism of newly absorbed vitamin A in the rat. *J. Lipid Res.*, **6**, 390–396.
6. Relas, H., Gylling, H. and Miettinen, T.A. (2000) Effect of stanol ester on postabsorptive squalene and retinyl palmitate. *Metabolism*, **49**, 473–478.
7. Blaner, W.S., Li, Y., Brun, P.J., Yuen, J.J., Lee, S.A. and Clugston, R.D. (2016) Vitamin a absorption, storage and mobilization. *Subcell. Biochem.*, **81**, 95–125.
8. van Bennekum, A.M., Kako, Y., Weinstock, P.H., Harrison, E.H., Deckelbaum, R.J., Goldberg, I.J. and Blaner, W.S. (1999) Lipoprotein lipase expression level influences tissue clearance of chylomicron retinyl ester. *J. Lipid Res.*, **40**, 565–574.
9. Quadro, L., Blaner, W.S., Salchow, D.J., Vogel, S., Piantedosi, R., Gouras, P., Freeman, S., Cosma, M.P., Colantuoni, V. and Gottesman, M.E. (1999) Impaired retinal function and vitamin A availability in mice lacking retinol-binding protein. *EMBO J.*, **18**, 4633–4644.
10. Episkopou, V., Maeda, S., Nishiguchi, S., Shimada, K., Gaitanaris, G.A., Gottesman, M.E. and Robertson, E.J. (1993) Disruption of the transthyretin gene results in mice with depressed levels of plasma retinol and thyroid hormone. *Proc. Natl. Acad. Sci.*, **90**, 2375–2379.
11. Noy, N., Slosberg, E. and Scarlata, S. (1992) Interactions of retinol with binding proteins: studies with retinol-binding protein and with transthyretin. *Biochemistry*, **31**, 11118–11124.
12. Bok, D. and Heller, J. (1976) Transport of retinol from the blood to the retina: an autoradiographic study of the pigment epithelial cell surface receptor for plasma retinol-binding protein. *Exp. Eye Res.*, **22**, 395–402.
13. Kawaguchi, R., Yu, J., Honda, J., Hu, J., Whitelegge, J., Ping, P., Wiita, P., Bok, D. and Sun, H. (2007) A membrane receptor for retinol binding protein mediates cellular uptake of vitamin a. *Science*, **315**, 820–825.
14. Sun, H. and Kawaguchi, R. (2011) The membrane receptor for plasma retinol-binding protein, a new type of cell-surface receptor. *Int. Rev. Cell Mol. Biol.*, **288**, 1–41.
15. Kawaguchi, R., Yu, J., Ter-Stepanian, M., Zhong, M., Cheng, G., Yuan, Q., Jin, M., Travis, G.H., Ong, D. and Sun, H. (2011) Receptor-mediated cellular uptake mechanism that couples to intracellular storage. *ACS Chem. Biol.*, **6**, 1041–1045.
16. Isken, A., Golczak, M., Oberhauser, V., Hunzelmann, S., Driever, W., Imanishi, Y., Palczewski, K. and von Lintig, J. (2008) RBP4 disrupts vitamin A uptake homeostasis in a STRA6-deficient animal model for Matthew-Wood syndrome. *Cell Metab.*, **7**, 258–268.
17. Kiser, P.D., Golczak, M. and Palczewski, K. (2014) Chemistry of the retinoid (visual) cycle. *Chem. Rev.*, **114**, 194–232.
18. Widjaja-Adhi, M.A.K. and Golczak, M. (2020) The molecular aspects of absorption and metabolism of carotenoids and retinoids in vertebrates. *Biochim. Biophys. Acta Mol. Cell Biol. Lipids*, **1865**, 158571.
19. Biesalski, H.K., Frank, J., Beck, S.C., Heinrich, F., Illek, B., Reifen, R., Gollnick, H., Seeliger, M.W., Wissinger, B. and Zrenner, E. (1999) Biochemical but not clinical vitamin A deficiency results from mutations in the gene for retinol binding protein. *Am. J. Clin. Nutr.*, **69**, 931–936.
20. Seeliger, M.W., Biesalski, H.K., Wissinger, B., Gollnick, H., Gielen, S., Frank, J., Beck, S. and Zrenner, E. (1999) Phenotype in retinol deficiency due to a hereditary defect in retinol binding protein synthesis. *Invest. Ophthalmol. Vis. Sci.*, **40**, 3–11.
21. Amengual, J., Zhang, N., Kemerer, M., Maeda, T., Palczewski, K. and Von Lintig, J. (2014) STRA6 is critical for cellular vitamin A uptake and homeostasis. *Hum. Mol. Genet.*, **23**, 5402–5417.
22. Ruiz, A., Mark, M., Jacobs, H., Klopfenstein, M., Hu, J., Lloyd, M., Habib, S., Tosha, C., Radu, R.A., Ghyselinck, N.B., Nusinowitz, S. and Bok, D. (2012) Retinoid content, visual responses, and ocular morphology are compromised in the retinas of mice lacking the retinol-binding protein receptor, STRA6. *Invest. Ophthalmol. Vis. Sci.*, **53**, 3027–3039.
23. Terra, R., Wang, X., Hu, Y., Charpentier, T., Lamarre, A., Zhong, M., Sun, H., Mao, J., Qi, S., Luo, H. and Wu, J. (2013) To investigate the necessity of STRA6 upregulation in T cells during T cell immune responses. *PLoS One*, **8**, e82808.
24. Berry, D.C., Jacobs, H., Marwarha, G., Gely-Pernot, A., O'Byrne, S.M., Desantis, D., Klopfenstein, M., Feret, B., Dennefeld, C., Blaner, W.S. *et al.* (2013) The STRA6 receptor is essential for retinol-binding protein-induced insulin resistance but not for maintaining vitamin a homeostasis in tissues other than the eye. *J. Biol. Chem.*, **288**, 24528–24539.
25. Kelly, M., Widjaja-Adhi, M.A., Palczewski, G. and von Lintig, J. (2016) Transport of vitamin A across blood-tissue barriers is facilitated by STRA6. *FASEB J.*, **30**, 2985–2995.

26. Paik, J., Vogel, S., Quadro, L., Piantedosi, R., Gottesman, M., Lai, K., Hamberger, L., Vieira Mde, M. and Blaner, W.S. (2004) Vitamin A: overlapping delivery pathways to tissues from the circulation. *J. Nutr.*, **134**, 276S–280S.
27. Zhong, M., Kawaguchi, R., Costabile, B., Tang, Y., Hu, J., Cheng, G., Kassai, M., Ribalet, B., Mancia, F., Bok, D. and Sun, H. (2020) Regulatory mechanism for the transmembrane receptor that mediates bidirectional vitamin A transport. *Proc. Natl. Acad. Sci. U. S. A.*, **117**, 9857–9864.
28. Amengual, J., Golczak, M., Palczewski, K. and von Lintig, J. (2012) Lecithin:retinol acyltransferase is critical for cellular uptake of vitamin A from serum retinol-binding protein. *J. Biol. Chem.*, **287**, 24216–24227.
29. Bouillet, P., Sapin, V., Chazaud, C., Messaddeq, N., Decimo, D., Dolle, P. and Chambon, P. (1997) Developmental expression pattern of Stra6, a retinoic acid-responsive gene encoding a new type of membrane protein. *Mech. Dev.*, **63**, 173–186.
30. Mustafi, D., Kevany, B.M., Bai, X., Golczak, M., Adams, M.D., Wynshaw-Boris, A. and Palczewski, K. (2016) Transcriptome analysis reveals rod/cone photoreceptor specific signatures across mammalian retinas. *Hum. Mol. Genet.*, **25**, 4376–4388.
31. Hennig, A.K., Peng, G.H. and Chen, S. (2008) Regulation of photoreceptor gene expression by Crx-associated transcription factor network. *Brain Res.*, **1192**, 114–133.
32. Moore, S.M., Skowronska-Krawczyk, D. and Chao, D.L. (2020) Targeting of the NRL pathway as a therapeutic strategy to treat retinitis pigmentosa. *J. Clin. Med.*, **9**, 2224.
33. Yokoyama, S. (2000) Molecular evolution of vertebrate visual pigments. *Prog. Retin. Eye Res.*, **19**, 385–419.
34. Maeda, T., Cideciyan, A.V., Maeda, A., Golczak, M., Aleman, T.S., Jacobson, S.G. and Palczewski, K. (2009) Loss of cone photoreceptors caused by chromophore depletion is partially prevented by the artificial chromophore pro-drug, 9-cis-retinyl acetate. *Hum. Mol. Genet.*, **18**, 2277–2287.
35. Kinoshita, J. and Peachey, N.S. (2018) Noninvasive electroretinographic procedures for the study of the mouse retina. *Curr. Protoc. Mouse Biol.*, **8**, 1–16.
36. Joachimsthaler, A. and Kremers, J. (2019) Mouse cones adapt fast, rods slowly in vivo. *Invest. Ophthalmol. Vis. Sci.*, **60**, 2152–2164.
37. Woodruff, M.L., Wang, Z., Chung, H.Y., Redmond, T.M., Fain, G.L. and Lem, J. (2003) Spontaneous activity of opsin apoprotein is a cause of Leber congenital amaurosis. *Nat. Genet.*, **35**, 158–164.
38. Jones, G.J., Cornwall, M.C. and Fain, G.L. (1996) Equivalence of background and bleaching desensitization in isolated rod photoreceptors of the larval tiger salamander. *J. Gen. Physiol.*, **108**, 333–340.
39. Fan, J., Woodruff, M.L., Cilluffo, M.C., Crouch, R.K. and Fain, G.L. (2005) Opsin activation of transduction in the rods of dark-reared Rpe65 knockout mice. *J. Physiol.*, **568**, 83–95.
40. Ridge, K.D., Abdulaev, N.G., Sousa, M. and Palczewski, K. (2003) Phototransduction: crystal clear. *Trends Biochem. Sci.*, **28**, 479–487.
41. Stojanovic, A. and Hwa, J. (2002) Rhodopsin and retinitis pigmentosa: shedding light on structure and function. *Recept. Channels*, **8**, 33–50.
42. Maeda, A., Maeda, T., Golczak, M. and Palczewski, K. (2008) Retinopathy in mice induced by disrupted all-trans-retinal clearance. *J. Biol. Chem.*, **283**, 26684–26693.
43. Chen, Y., Palczewska, G., Mustafi, D., Golczak, M., Dong, Z., Sawada, O., Maeda, T., Maeda, A. and Palczewski, K. (2013) Systems pharmacology identifies drug targets for Stargardt disease-associated retinal degeneration. *J. Clin. Invest.*, **123**, 5119–5134.
44. Tanumihardjo, S.A., Russell, R.M., Stephensen, C.B., Gannon, B.M., Craft, N.E., Haskell, M.J., Lietz, G., Schulze, K. and Raiten, D.J. (2016) Biomarkers of nutrition for development (BOND)-vitamin A review. *J. Nutr.*, **146**, 1816S–1848S.
45. Sommer, A. and Vyas, K.S. (2012) A global clinical view on vitamin A and carotenoids. *Am. J. Clin. Nutr.*, **96**, 1204S–1206S.
46. Dowling, J.E. and Wald, G. (1958) Vitamin A deficiency and night blindness. *Proc. Natl. Acad. Sci. U. S. A.*, **44**, 648–661.
47. Hu, Y., Chen, Y., Moiseyev, G., Takahashi, Y., Mott, R. and Ma, J.X. (2011) Comparison of ocular pathologies in vitamin A-deficient mice and RPE65 gene knockout mice. *Invest. Ophthalmol. Vis. Sci.*, **52**, 5507–5514.
48. Rohrer, B., Lohr, H.R., Humphries, P., Redmond, T.M., Seeliger, M.W. and Crouch, R.K. (2005) Cone opsin mislocalization in Rpe65−/− mice: a defect that can be corrected by 11-cis retinal. *Invest. Ophthalmol. Vis. Sci.*, **46**, 3876–3882.
49. Znoiko, S.L., Rohrer, B., Lu, K., Lohr, H.R., Crouch, R.K. and Ma, J.X. (2005) Downregulation of cone-specific gene expression and degeneration of cone photoreceptors in the Rpe65−/− mouse at early ages. *Invest. Ophthalmol. Vis. Sci.*, **46**, 1473–1479.
50. Samardzija, M., Tanimoto, N., Kostic, C., Beck, S., Oberhauser, V., Joly, S., Thiersch, M., Fahl, E., Arsenijevic, Y., von Lintig, J. *et al.* (2009) In conditions of limited chromophore supply rods entrap 11-cis-retinal leading to loss of cone function and cell death. *Hum. Mol. Genet.*, **18**, 1266–1275.
51. Vogel, S., Piantedosi, R., O'Byrne, S.M., Kako, Y., Quadro, L., Gottesman, M.E., Goldberg, I.J. and Blaner, W.S. (2002) Retinol-binding protein-deficient mice: biochemical basis for impaired vision. *Biochemistry*, **41**, 15360–15368.
52. Imanishi, Y., Gerke, V. and Palczewski, K. (2004) Retinosomes: new insights into intracellular managing of hydrophobic substances in lipid bodies. *J. Cell Biol.*, **166**, 447–453.
53. Chen, Y., Clarke, O.B., Kim, J., Stowe, S., Kim, Y.K., Assur, Z., Cavalier, M., Godoy-Ruiz, R., von Alpen, D.C., Manzini, C. *et al.* (2016) Structure of the STRA6 receptor for retinol uptake. *Science*, **353**, aad8266.
54. Pyakurel, A., Balmer, D., Saba-el-Leil, M.K., Kizilyaprak, C., Daraspe, J., Humbel, B.M., Voisin, L., le, Y.Z., von Lintig, J., Meloche, S. and Roduit, R. (2017) Loss of extracellular signal-regulated kinase 1/2 in the retinal pigment epithelium leads to RPE65 decrease and retinal degeneration. *Mol. Cell. Biol.*, **37**, e00295–e00217.
55. Redmond, T.M., Poliakov, E., Yu, S., Tsai, J.Y., Lu, Z. and Gentleman, S. (2005) Mutation of key residues of RPE65 abolishes its enzymatic role as isomerohydrolase in the visual cycle. *Proc. Natl. Acad. Sci. U. S. A.*, **102**, 13658–13663.
56. Redmond, T.M., Yu, S., Lee, E., Bok, D., Hamasaki, D., Chen, N., Goletz, P., Ma, J.X., Crouch, R.K. and Pfeifer, K. (1998) Rpe65 is necessary for production of 11-cis-vitamin A in the retinal visual cycle. *Nat. Genet.*, **20**, 344–351.
57. von Lintig, J. and Vogt, K. (2000) Filling the gap in vitamin A research. Molecular identification of an enzyme cleaving beta-carotene to retinal. *J. Biol. Chem.*, **275**, 11915–11920.
58. Gao, S., Parmar, T., Palczewska, G., Dong, Z., Golczak, M., Palczewski, K. and Jastrzebska, B. (2018) Protective effect of a locked retinal chromophore analog against light-induced retinal degeneration. *Mol. Pharmacol.*, **94**, 1132–1144.
59. Surya, A., Foster, K.W. and Knox, B.E. (1995) Transducin activation by the bovine opsin apoprotein. *J. Biol. Chem.*, **270**, 5024–5031.
60. Wald, G. and Brown, P.K. (1953) The molar extinction of rhodopsin. *J. Gen. Physiol.*, **37**, 189–200.